CLAS-NOTE 95-026

CLAS Čerenkov Detector Simulations and Design Analysis

Alexander V. Vlassov, Mikhail V. Kossov

Institute of Theoretical and Experimental Physics
B.Cheremushkinskaya, 25, Moscow, 117259 Russia

Volker D. Burkert

CEBAF, 12000 Jefferson Avenue, Newport News,
Virginia 23606,USA

November 28, 1995

1 Overview.

The Čerenkov detectorrs will be used in CLAS to identify electrons and to separate them from other charged particles, mostly pions.

A GEANT[1] - based program package was developed to study the Čerenkov detector response - *CC* package [2].
This report contains a short description of this package , including recent improvements, and results of the Čerenkov detector response analysis mostly based on simulations using this package.

The main items covered in this report are:

- Software support of Čerenkov detector design.
  - Motivation for the choice of radiator gas.
  - Implemention of additional mirrors.
  - Optimization of mirror positions for maximum electron detection efficiency
  - The required accuracy for the mirror positioning.

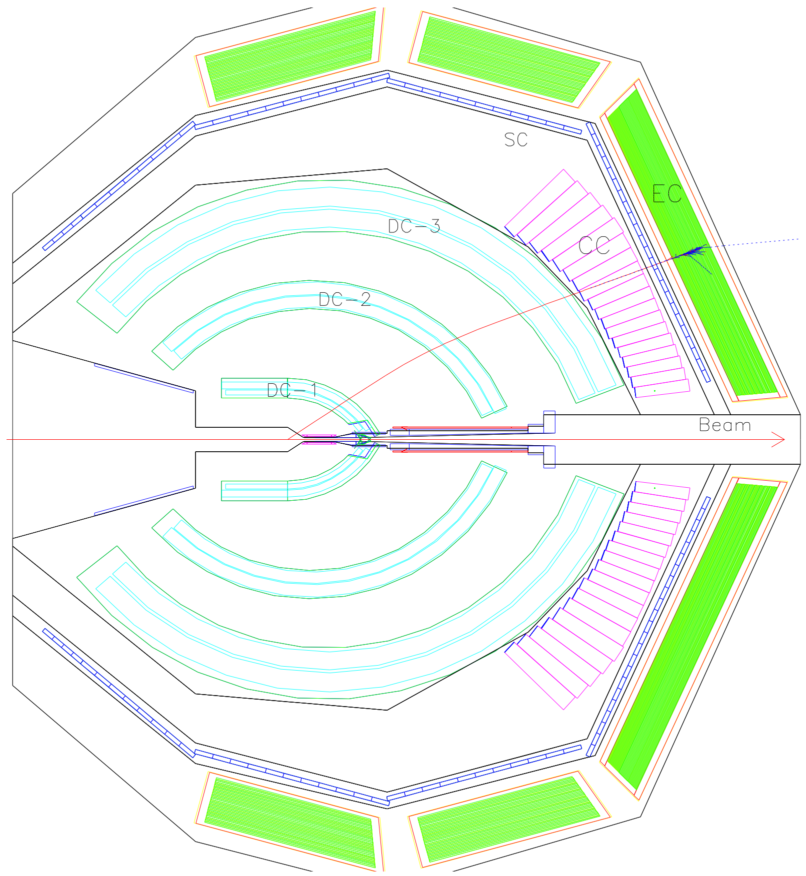

Figure 1: Scheme of CLAS

- Alignment procedure for the mirror system.
- Simulations of trigger schemes.

- Software support for physics proposals.
  - Detailed estimates of electron detection efficiencies.
  - π/e rejection.
  - Background.

This package is ready to be used as part of the GEANT description of CLAS **(GSIM)** for the study of user-defined exclusive electron - nuclear reactions.

2 Main concepts of *CC* package

2.1 CLAS Čerenkov detector

The Čerenkov detector is positioned between the Drift Chamber Region 3 (*DC-3*) and the Time Of Flight Scintillator (*SC*) system (see Fig. 1). It covers the region of polar angles $\theta = 7^o \div 48^o$ in the forward direction. Each of the 6 sectors of CLAS consists of 18 segments.

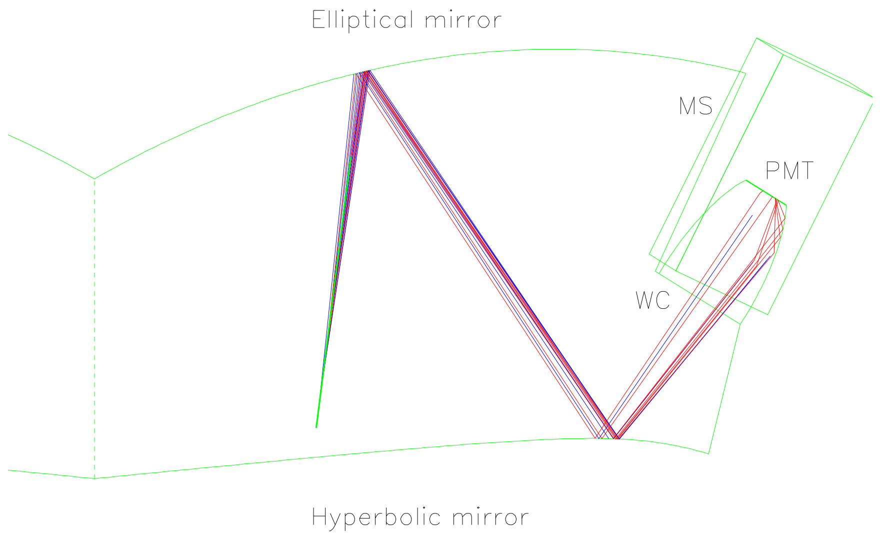

Figure 2: Simplified ray tracing scheme in one Čerenkov detector segment

A simplified scheme of ray-tracing inside the Čerenkov segments is presented in Fig. 2

The segments are symmetric with respect to the *middle plane*, and consist of two elliptical and two hyperbolic mirrors, and Winston cones (*WC*), and two PhotoMultiplier tubes (*PMT*).

A fast particle with velocity

$$v > \frac{c}{n} \ ,$$

where n is the gas refraction index, produces Čerenkov light in a narrow cone in forward direction. This light is focused by the elliptical and hyperbolic mirrors and the *WC* onto the *PMT* cathode window.

The goal of the *CC* package, as part of the GEANT-based description of CLAS, is to simulate the response of the Čerenkov detector.

2.2 Definitions and some terminology

Three main reference systems are used for the detector elements description :

- *MAster Reference System - MARS* : origin is in the target center, beam direction along Z axis, vertical line along Y axis.

- *Sector Reference System* is connected with one sector of CLAS with the origin in the target center. A (X,Z) plane divides the Sector in two symmetric parts. This plane is named *Sector middle plane* or *middle plane*. The Z axis is parallel to the Z axis of the MAster Reference System.

- *Segment Reference System* is connected with each CC segment. The origin is in the target center, the Y axis lies in the *Sector middle plane* and crosses the target and the center of the CC segment. The X axis is perpendicular to the middle plane. A (X,Y) plane crosses the centers of the mirrors and the Winston Cones, and is called the *Segment median plane* or *Median plane*.

  This reference system is convenient for the description of mirror shapes and for the ray-tracing inside the segment.

2.3 Structure of the *CC* package

The full description of ALL software packages structure can be found in the description of the CLAS GEANT simulation package **GSIM**.

The main idea is that the structure of every package, concerned with different detector types (*DC, CC, SC, EC* etc) follows the GEANT philosophy :

- There are some initialization subroutines (*CCINIT*) to define volumes, materials, media, to read geometry parameters from a file or BOS banks, to define control flow cards, etc..

- The trajectory of each particle , which reached a sensitive volume , is divided into a number of **steps** and a **step** routine is called (*CCSTEP*). At each call the coordinates at the beginning and at the end of the **step**, the particle and medium characteristics, etc. are acceptable. This routine is used to define the response from this part of the particle trajectory and to store it (say, in *HITS* structure).

- After ALL tracks in the event are processed, the *DIGI* routine is called (*CCDIGI*), which calculates the *CC* response for the total event. It uses the information on both primary and secondary tracks. This response is stored in the *DIGI* structure, or in a special BOS bank - to reproduce the same format as proposed for *ONLINE* events.

- Some routines may be called at the end of each event (e.g.*CCOUT*)

2.4 Physics aspects of the ray-tracing procedure

The Čerenkov detector response is calculated by a special ray-tracing procedure (*CCVPHO*).

The main features of this procedure are:

- For every **step** the effective number of photons $N_{p.e.}$ is calculated. This number is proportional to the **step** length and depends on the Čerenkov gas refraction index $n(E)$, its transparency as a function of wavelength, the average quantum efficiency (ε_{pmt}) of the PhotoMultiplier Tubes (PMT) and the particle velocity. This is discussed in sections **3.1** and **6.0** in more detail.

- Ray-tracing is performed for each effective photon. In case the photon reaches the PMT, it generates ONE additional photo-electron for this PMT. Possible losses due to less then perfect reflection off mirrors and Winston cones, absorption on the surface of magnetic shields or support frames, are taken into account.

- The Ray-tracing subroutine uses realistic shapes and positions of all mirrors, Winston cones, magnetic shields and support frames. Particle trajectories can begin at any point inside the Čerenkov detector - this is important in case of secondary particle production.

- The Čerenkov gas, elliptical and hyperbolic mirrors, magnetic shields, Winston cones are described in GEANT also as different **materials**. This is important for an accurate estimation of the detection efficiency of slow particles.

3 Choice of the radiator gas for the Čerenkov detector

The choice of the radiator gas has to take into account two requirements :

- High electron detection efficiency.

- Low pion detection efficiency.

Initially Freon-12 was assumed to be the gas of choice for the Čerenkov detector. We will therefore compare gas properties relative to Freon-12.

3.1 Mean number of photo-electrons.

The mean number of generated photo-electrons depends on the index of refraction of the radiator gas, its transmissivity , especially at short wavelengths, quantum efficiency of PMT, and mirror reflectivity. The intensity and spectrum of photons is given by the Frank-Tamm relation :

$$\frac{dN_\gamma}{dE} = (\frac{\alpha}{\hbar c})Z^2 L[1-(\frac{1}{n(E)\beta})^2] \ ,$$

where Z is the particle charge, $n(E)$ is the index of refraction, L is particle trajectory length and $(\frac{\alpha}{\hbar c}) = 370 eV^{-1}cm^{-1}$. The expected number of obtained photoelectrons is then

$$N_{ph.e.} = \int \frac{dN_\gamma}{dE}\varepsilon(E)dE \ ,$$

where $\varepsilon(E)$is the detection efficiency of the photons with energy E. $\varepsilon(E)$ depends on Čerenkov gas transparency, reflection losses, quantum sensitivity of PMT and probability to miss this PMT because of geometry factors.

3.2 Detector efficiency dependence on the gas refraction index

Table 1. shows the expected mean number of photoelectrons for different gases, due to the difference in index of refraction. The value for Freon-12 is about 6.0 ph.e., however, this number varies significantly from point to point, - Fig. 3 shows the number of detected photoelectrons for an initial electron energy of 0.8 GeV as a function of the polar (*Theta*) and azimuthal (*Phi*) angles.

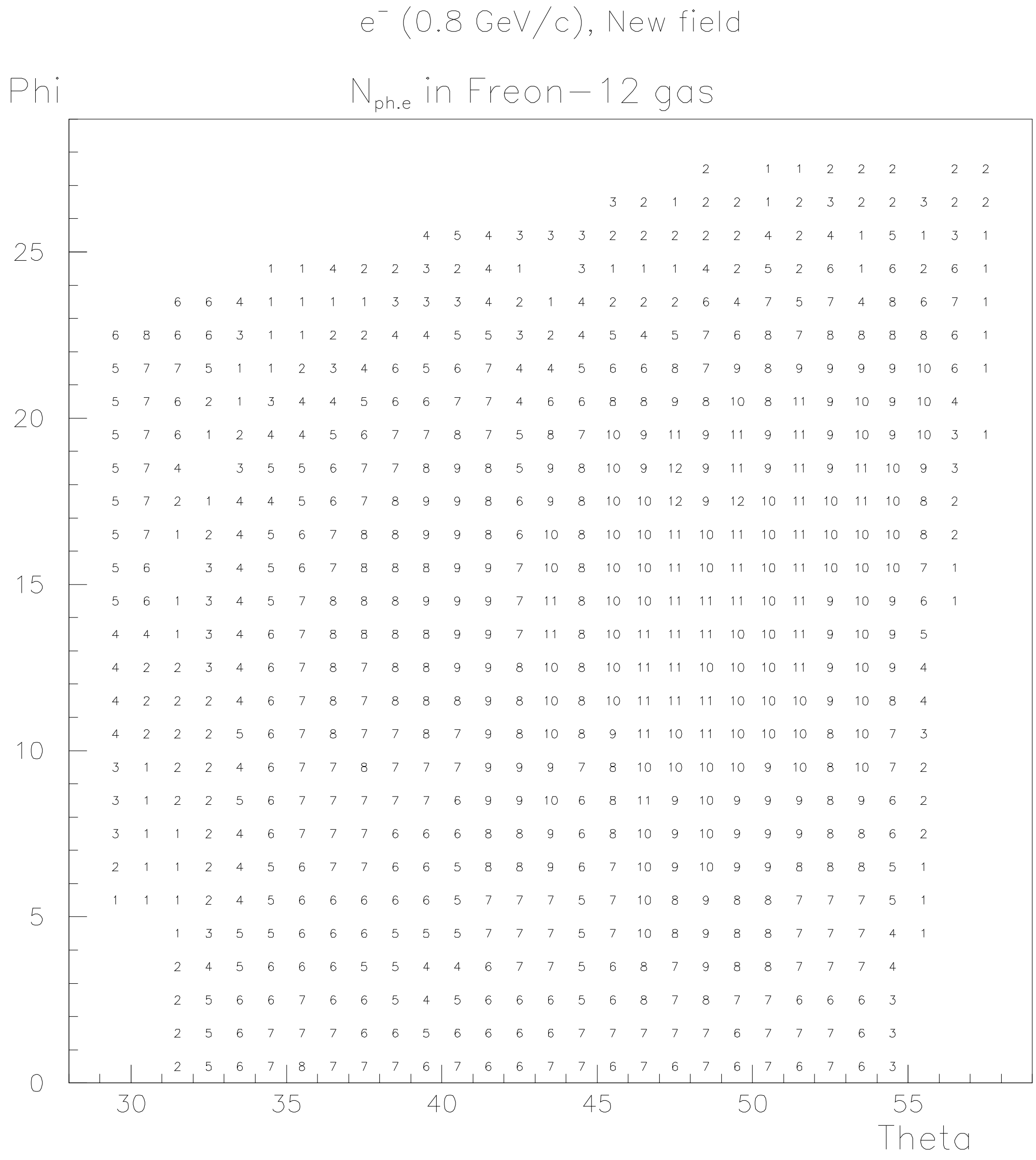

Figure 3: Mean numbers of photoelectrons in Freon-12 gas versus angles *Theta* and *Phi*. Initial energy of electrons is 0.8 GeV.

Gas name	Chemical composition		Refr. index	Estimated $N_{ph.e.}$	
Freon 12	CCl_2F_2	[3]	1.001080	6.00	(1.00)
	CCl_2F_2	[4]	1.001127	6.26	(1.04)
Freon 13 B1	CCl_2F_2	[5]	1.000864	4.80	(0.80)
Freon 13	$CClF_3$	[4]	1.000782	4.34	(0.72)
Freon 114	$C_2Cl_2F_4$	[6]	1.0014 [7]	7.78	(1.30)
Freon 318	C_4F_8	[4]	1.001285	7.14	(1.19)
Perfluorobutane	C_4F_{10}	[8, 9]	1.00153	8.50	(1.42)
Perfluoropentane	C_5F_{12}	[8, 9]	1.00172	9.56	(1.59)

Table 1: **Indices of refraction for various radiate gases and estimated mean number of photoelectrons.**

The coefficient in parentheses is the ratio to the Freon-12 value. One can see that, for example, Perfluorobutane (C_4F_{10}) provides additional 2.5 photoelectrons due to the index of refraction alone.

To estimate the effect of one additional photo-electron, we consider the electron detection efficiency dependence on $< N_{ph.e.} >$ (ξ).

In simple cases, when it is possible to neglect geometry factors, the number of detected photoelectrons is distributed according to Poisson's law :

$$p(k) = e^{-\xi} \cdot \frac{\xi^k}{k!}$$

We define the detection threshold as the minimum number of photoelectrons necessary to detect a signal from the *PMT*. The detection efficiency for a one-photo-electron threshold is

$$(1 - \eta_e) = 1 - e^{-\xi}$$

For η_e to be less than 10^{-3} , ξ should be greater than 7. Actually the "real" distribution is wider than the Poisson distribution, and the probability to obtain zero photoelectrons is greater than the value estimated using Poisson's law. In order to obtain a value of 10^{-3} for the electron inefficiency, we need an additional 2-3 photoelectrons. If one is forced to raise the threshold to a few photoelectrons, for example due to background events, the mean number of photoelectrons should be even higher.

3.3 Transparency of radiator gases

Another important property of the gas is its optical transparency, especially in the short wavelength region. The reason is that the number of Čerenkov photons behaves like $n_c \sim \frac{1}{\lambda}$, where λ is the photon wavelength.

The transparency of various gases is shown in Fig. 4. Carbofluoride data are extracted from [9], Freon data from [10].

Gas formula	γ threshold	Density g/l	Relative π efficiency
CCl_2F_2	21.5	4.93	1.0
$CClF_3$	25.3	5.01	0.86
C_4F_8	19.7	8.92 [4]	1.98
C_4F_{10}	18.1	9.935 [11]	2.42

Table 2: Estimation of π-meson detection efficiency for different gases

Obviously, the transparency of C_4F_{10} is much better than that of Freon-12. The main gain is at $\lambda = 200 \div 240nm$. At shorter wavelengths, the mirror reflectivity is low. This wavelength region therefore adds little to the photon detection efficiency.

C_5F_{12} gas also has good transparency and a large index of refraction, however, its boiling point is as high as 40^oC, which makes it difficult to use in CLAS.

3.4 Efficiency of pion detection.

Although C_4F_{10} is much better than Freon-12 for electron detection, the crucial question is how it performs for pion rejection. Preliminary estimations[2] of the pion detection efficiency show that it is sufficiently small for Freon-12 gas.

An important mechanism for the detection of slow (with velocity under the Čerenkov gas threshold) pions is due to the detection of fast knock-on electrons.

Fig. 5 shows the number of knock-on electrons with energies above threshold as a function of the threshold energy. This value is approximately proportional to the probability of pion detection. Thresholds for different gases are shown as well.

The number of knock-on electrons also depend on the gas density, which varies significantly for different gases.

Table 2. shows the threshold γ - factor: $\gamma = \frac{1}{\sqrt{1-v^2}}$, gas density and estimated value of relative pion detection efficiency with respect to Freon-12 gas. The pion detection efficiency is discussed in more detail in section **6.3**.

We conclude that C_4F_{10} can be used as the radiator gas for the CLAS Čerenkov detector.

Another factor which affects the performance of the detector is light cone opening angle, which is greater for C_4F_{10} than for Freon-12. Fig. 6 shows the difference in $N_{ph.e}$ for C_4F_{10} and Freon-12 as a function of *Theta* and *Phi*, computed using the *CC* package.

We note the net gain of $2 \div 4$ additional photoelectrons in case of C_4F_{10} gas for the most part of the sensitive region. This is in good agreement with estimations from Table 1.

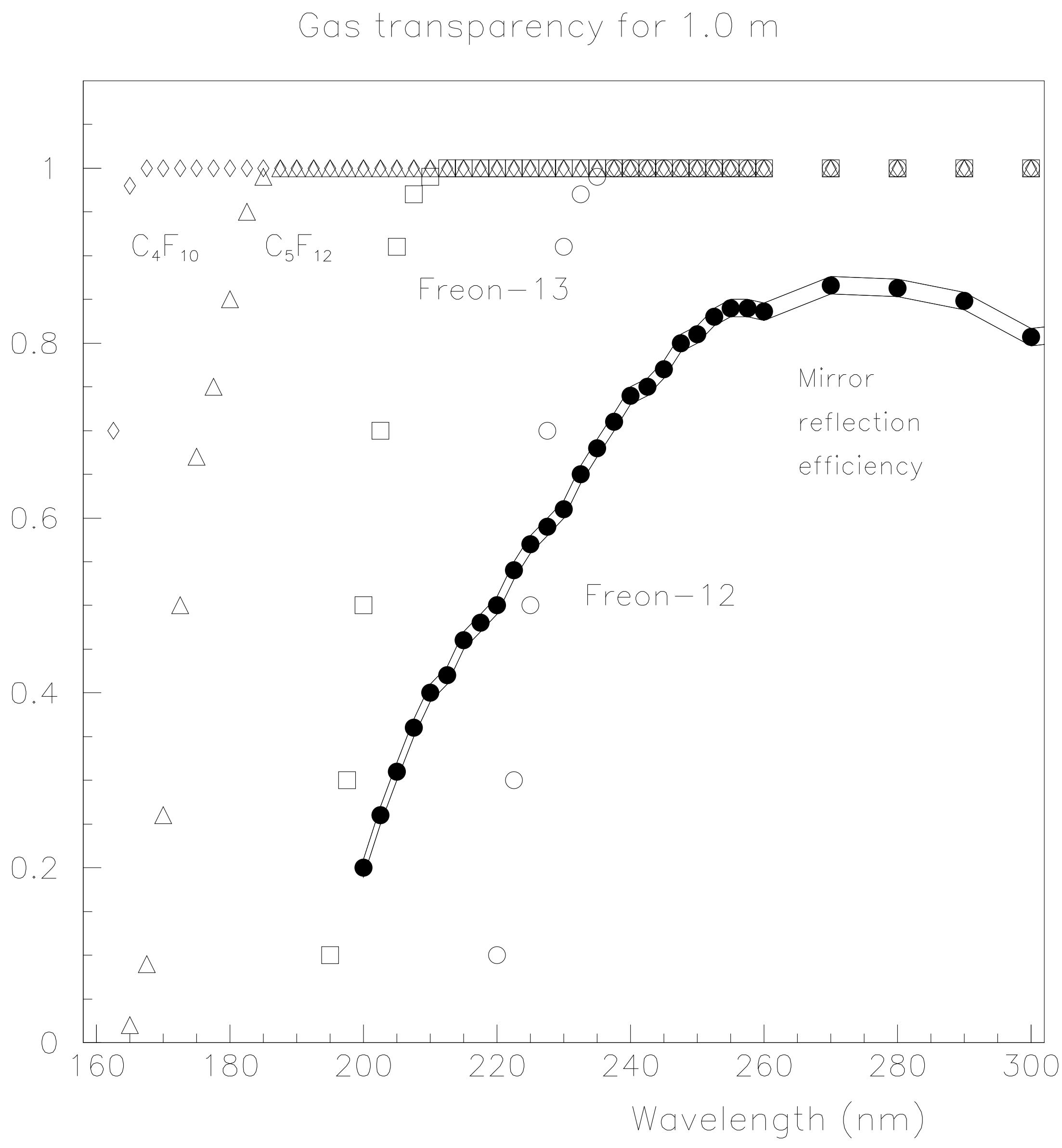

Figure 4: Wavelength dependence of gas transparencies. Black circles show the estimated mirror reflectivity for aluminized mylar coated with MgF_2.

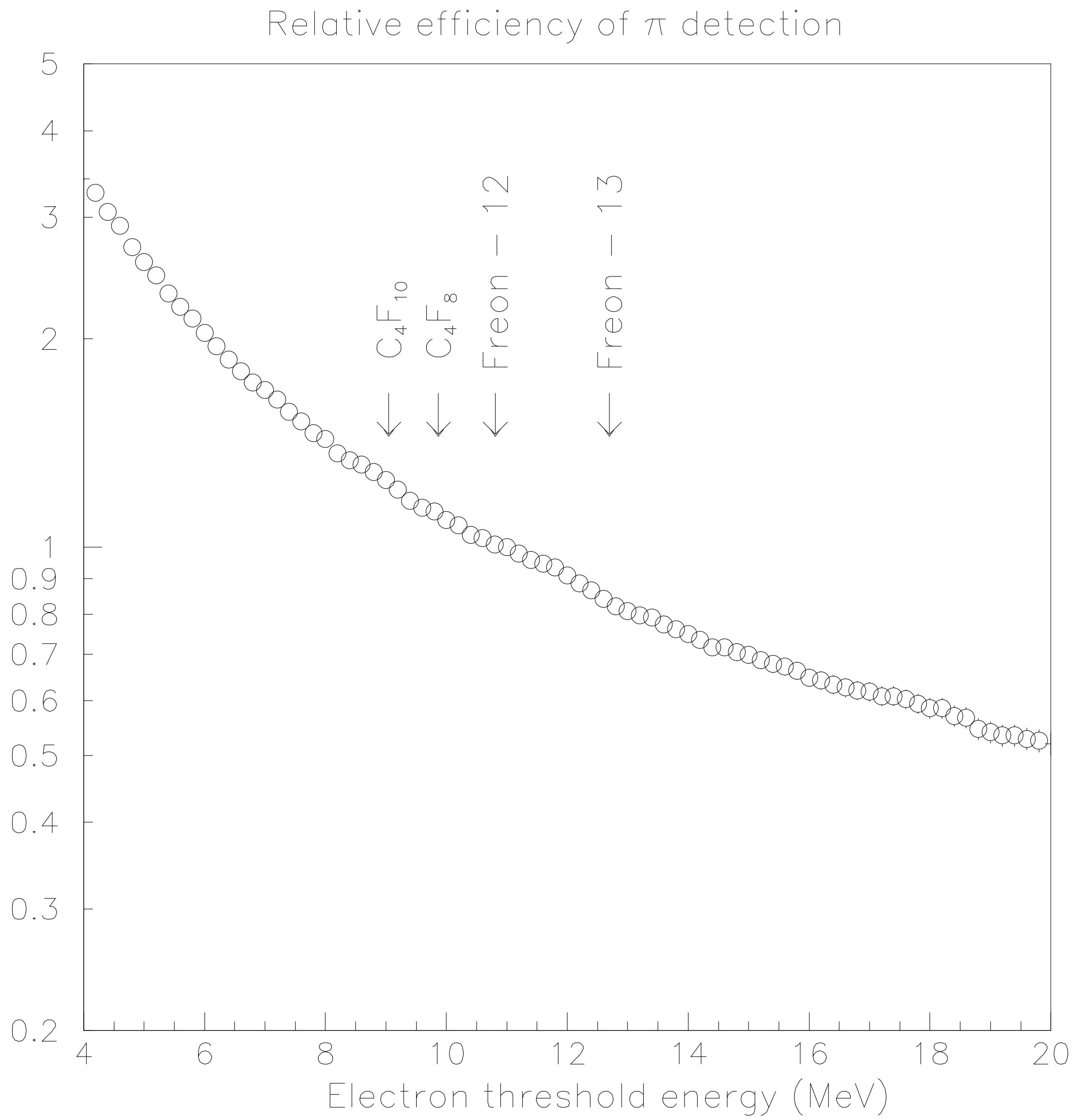

Figure 5: Energy distribution of secondary electrons in $\pi - A$ interactions

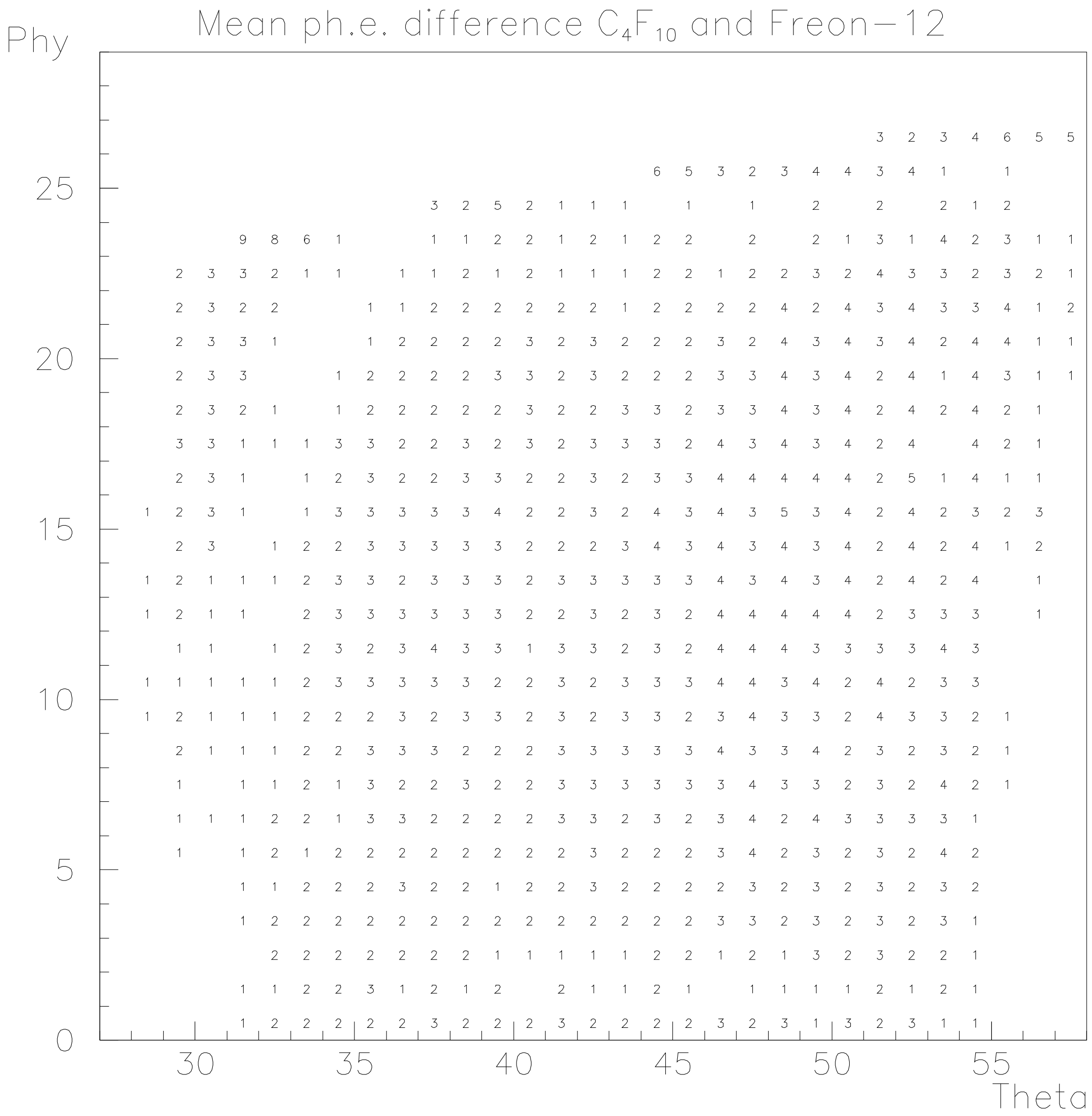

Figure 6: Difference in mean number of photo-electrons for C_4F_{10} and Freon-12 gases as a function of *Theta* and *Phi* for 0.8 GeV electrons.

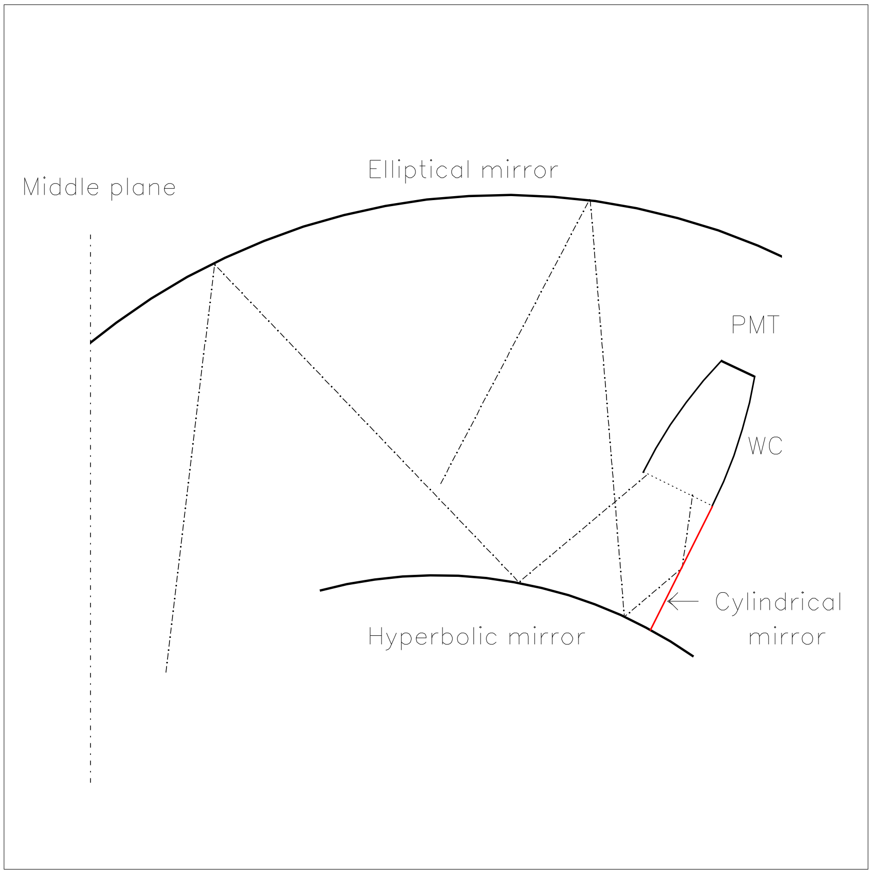

Figure 7: Scheme of Čerenkov photon ray-tracing

4 Design improvements

4.1 Cylindrical mirror implemention

Ray-tracing simulations show that some photons miss the PMT because of the limited size of the WC opening (see Fig. 7). This deficiency can be remedied by adding another mirror to the system.

In order to define the proper shape of this mirror, two different geometries were implemented in the *CC* package code - flat and cylindrical. It was found that the cylindrical mirror option resulted in a slightly larger $N_{ph.e.}$. It also proved to be more convenient to fabricate and to attach to the *WC* window.

Fig. 8 shows the estimated gain in $N_{ph.e.}$ from this modification.

4.2 Optimization of the mirror positions

In order to optimize the mirror positions a number of constraints had to be considered :

- The detection efficiency should be optimized for high momentum electrons (3.0 GeV/c)

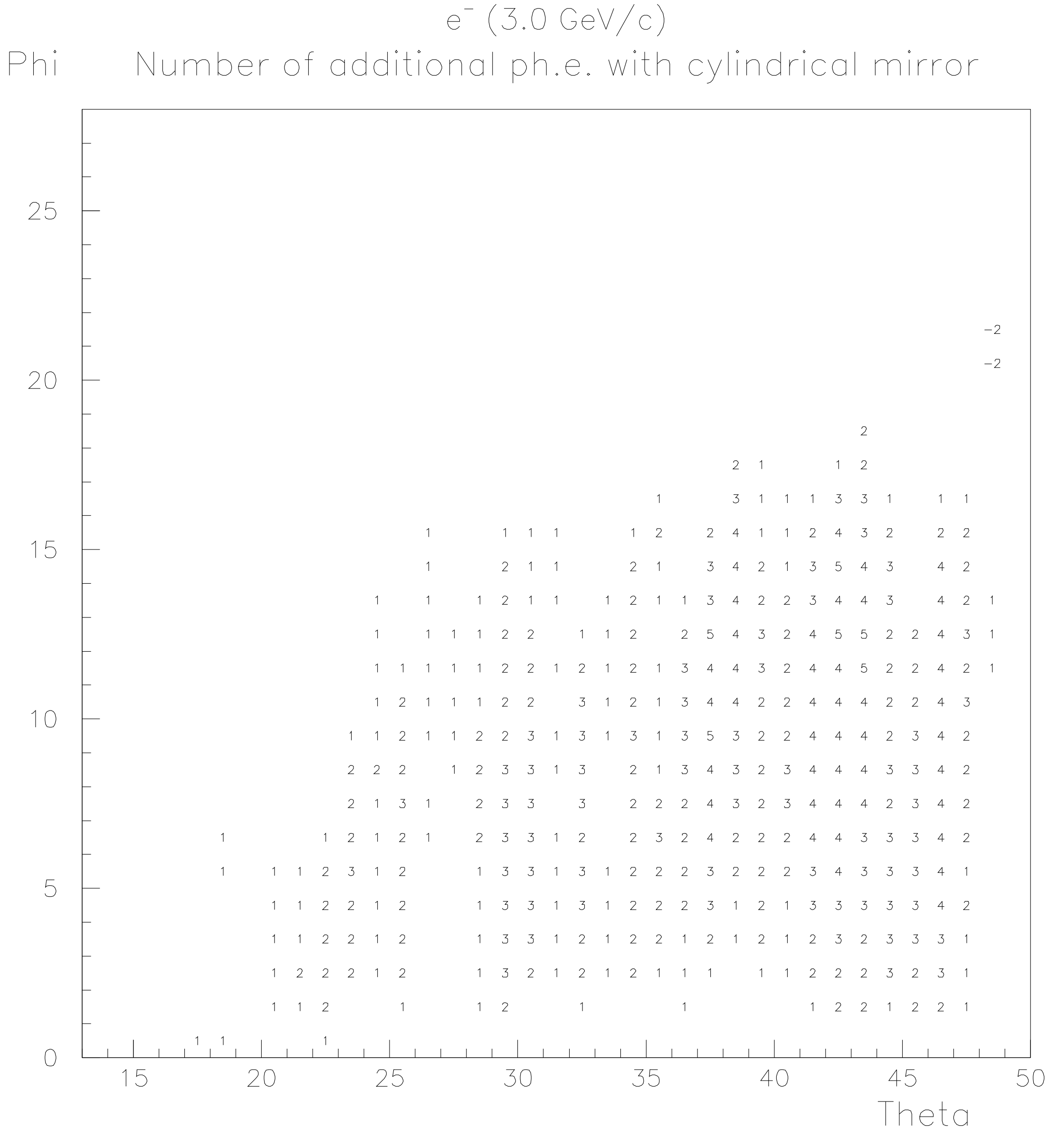

Figure 8: Number of additional photo-electrons due to cylindrical mirror

- In order to increase the electron efficiency for low momentum electrons ($\leq 0.8 GeV$) part of elliptical mirrors near the *middle plane* were made flat. This resulted in a diminished *near-middle-plane* efficiency for high energy electrons. We had to address the question how to keep the efficiency sufficiently high.

- Neighbouring mirrors overlap - they are wider than the distance between their centers. This was done to make sure that there will be no gaps between them. The goal was to minimize the interference of neighbouring mirrors.

The sensitivity of the Čerenkov detector optics to the exact mirror orientation can be seen in Fig. 9, which displays $N_{ph.e}$ as a function of the azimuthal angle *Phi* for fixed polar angle *Theta*. Different symbols represent different rotation angles for the elliptical mirrors. The elliptical mirrors are rotated around the center of the bracket, positive direction is when the away side of the mirror is closer to the target.

Fig. 9a and 9b represents the case with additional cylindrical mirrors, Fig 9c and 9d - without it.

One can see, that

1. 1^o deviation in the elliptical mirror angle results in the loss of 2 - 3 photo-electrons. Such a loss would be unacceptable (see chapter 3.2). Therefore, the angle deviation should be smaller then $\approx 0.5^o$.

2. The behavior at small *Phi* angles is different from the behavior at large *Phi*. Optimization requires finding a compromise position between highest $N_{ph.e}$ and high efficiency near the *middle plane*.

3. Comparing figures $9a), 9b)$ with $9c), 9d)$ shows that the optimal position depends on whether the additional mirrors are implemented or not.

4. The additional cylindrical mirrors not only increase $N_{ph.e.}$ but also reduce the sensitivity to the deviation from the ideal mirror position. [Compare Fig. 9a) and Fig. 9c)]

4.3 Mirrors alignment procedure

A special procedure was developed for aligning the mirrors. This procedure is based on the ray-tracing for the optimized mirror positions. The alignment scheme is presented in Fig. 10.

This procedure includes :

- A laser device is installed in the nominal target position. It can be rotated in two perpendicular planes.

- A transparent screen is stretched along the *segment median plane* perpendicular to the straight line from the target to the center of the screen. Therefore the center line of the screen and the center line of the calculated mirror position are in the same plane.

- The elliptical mirror will be aligned first, before the hyperbolic mirror is installed.

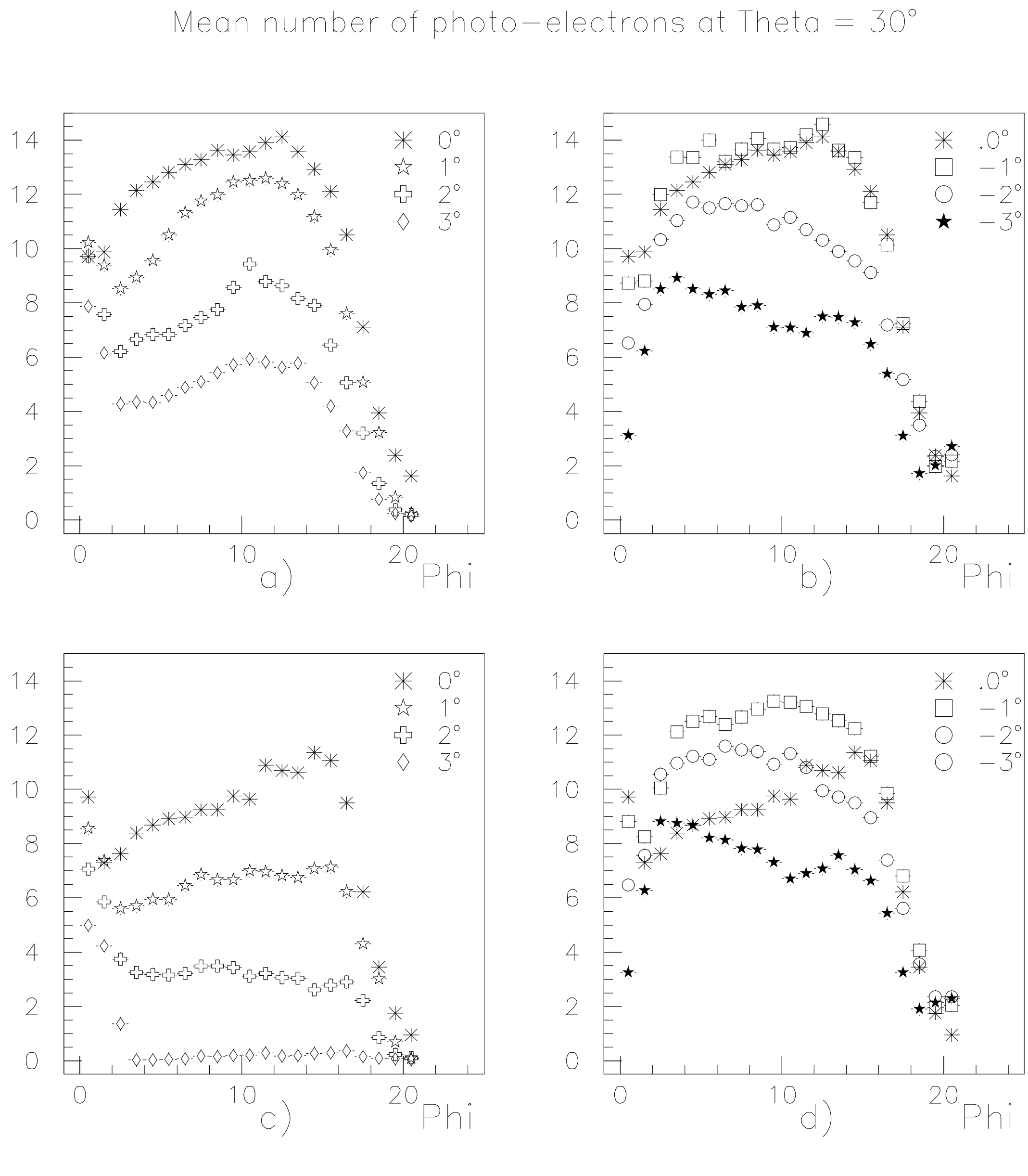

Figure 9: Čerenkov detector sensitivity to a rotation of the elliptical mirrors. (See text)

- The laser beam is directed to the center line of the elliptical mirror. Its crossing with the transparent screen is visible as a spot (S_1). A second spot on the screen indicates the position of the reflected light (S_2).

- The mirror will be aligned so that both S_1 and S_2 will be on the center line of the screen. This ensures that the mirror surface is perpendicular to the *segment median plane*.

- The distance from S_2 to the *middle plane* is calculated as a function of the distance from S_1 to the middle plane for the optimized mirror position, and stored in an **alignment table**.

- By rotating the mirror around its attachment point the position of S_2 can be adjusted according to the **alignment table**.

- After completion of the above procedure, the hyperbolic mirror is attached. The laser light is reflected from the hyperbolic mirror and entered the WC window (S_3) , which is covered by another screen. The "theoretical position" of S_3 with respect to the center of WC window is also stored in the **alignment table** as a function of the distance from S_1 to the *middle plane*.

As was shown in chapter 4.2 the deviation of S_2 position should not exceed a few millimeters. The center of the spot can be defined with an accuracy of $1 \div 2$ mm for the light reflected off the elliptical part of mirror, and $3 \div 5$ mm for light reflected off the flat part.

5 Trigger estimations

The Čerenkov detector response will be used in the level **1** trigger. One of the questions that arise is the optimal number of neighbouring Čerenkov detector elements (PMTs) that should be added in a pre-trigger scheme. This number should be large enough not to diminish the electron detection efficiency and small enough to allow selection of certain polar angle regions (e.g. to select high Q^2 or low Q^2 events).

It is natural to sum signals from both PMT of each segment, since one electron can produce a signal in both PMTs.

Four trigger schemes were analyzed:

1. Just one segment in a group.

2. Two segments in a group.

   Group # 1 includes segments 1 & 2;

   Group # 2 includes segments 2 & 3;

   ....

   Group # 17 includes segments 17 & 18;

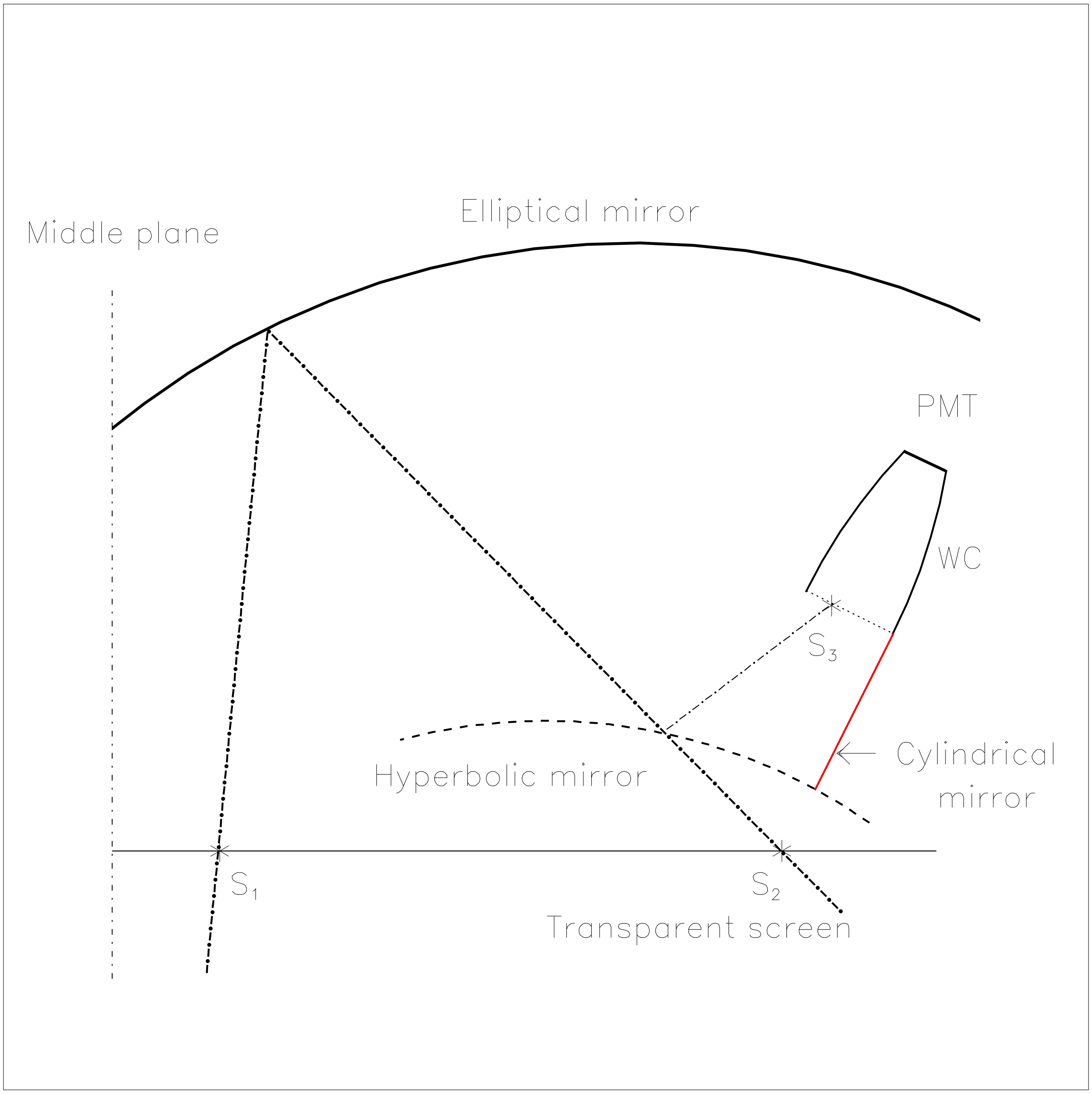

Figure 10: Scheme of mirrors alignment

3. Three segments in a group.

   Group # 1 includes segments 1 & 2 & 3

   Group # 2 includes segments 3 & 4 & 5

   ....

   Group # 9 includes segments 17 & 18;

4. Four segments in a group.

   Group # 1 includes segments 1 & 2 & 3 & 4

   Group # 2 includes segments 3 & 4 & 5 & 6

   ....

   Group # 8 includes segments 15 & 16 & 17 & 18

The groups overlap so that there is always at least one group which contains the total number of photo-electrons, generated by the electron.

How many segments should be added depends on the electron momentum. For low momentum electrons this number will be larger.

Fig 11 a) shows the distribution of the number of hit CC segments for electrons of 0.8 GeV energy. Typically $1 \div 3$ detector segments fire. Figures 11 b), 11 c) and 11 d) show a comparison of different trigger schemes for few different PMT detection threshold (in terms of photoelectrons). The trigger efficiency is defined here as the ratio of events satisfying the trigger condition and the number of events with at least one photoelectrons produced.

It is clear from the figure, that $3 \div 4$ segments in a group are sufficient - there is virtually no difference between the TRIG=3 and TRIG=4 schemes.

6 Particle detection efficiency estimations

As shown in chapter 3.1, the particle detection efficiency depends on a number of factors, such as gas refraction index, its transparency, mirror reflection efficiency, PMT quantum efficiency and mirror optics.

In order to separate geometry factors from gas and mirror properties, the number of effective photons ν_γ was calculated.

$$\nu_\gamma = \int \frac{dN_\gamma}{dE} \varepsilon(E) dE = \int \frac{dN_\gamma}{dE} \varepsilon_{PMT}(E) \varepsilon_{trans}(E, L_\gamma) \varepsilon_{refl}(E, N_{ref}) dE$$

Here $\varepsilon_{trans}(E, L_\gamma)$ is the radiator gas transmissivity for a photon trajectory length L_γ, $\varepsilon_{refl}(E, N_{ref})$ is the mirror reflectivity for N_{ref} reflections, and $\varepsilon_{PMT}(E)$ is the PMT quantum efficiency.

Fig. 12 shows the PMT quantum efficiency as a function of the wavelength (stars). Open circles and open triangles represent the minimum and maximum quantum efficiencies of a

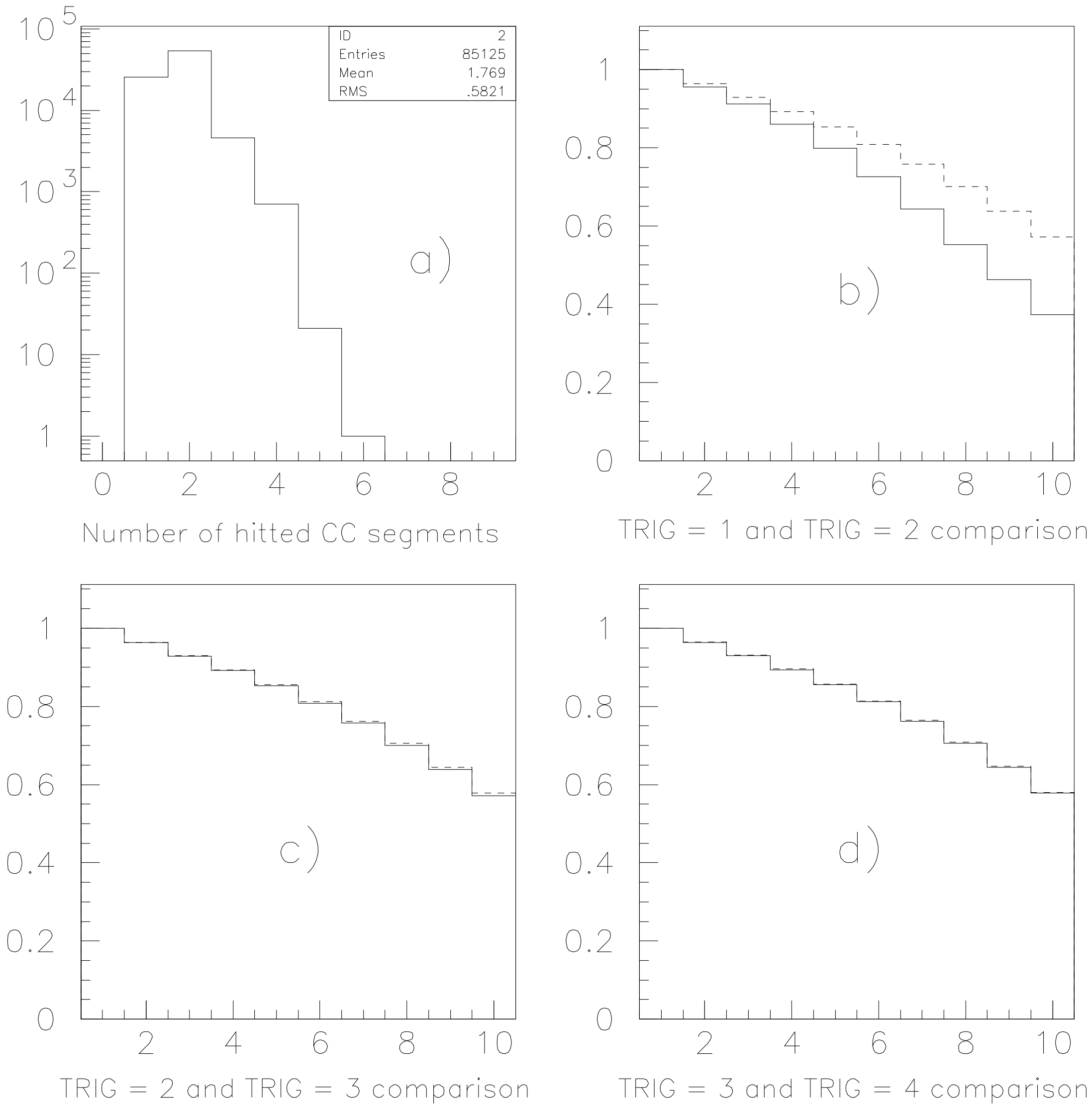

Figure 11: Comparison of trigger efficiencies for different schemes.

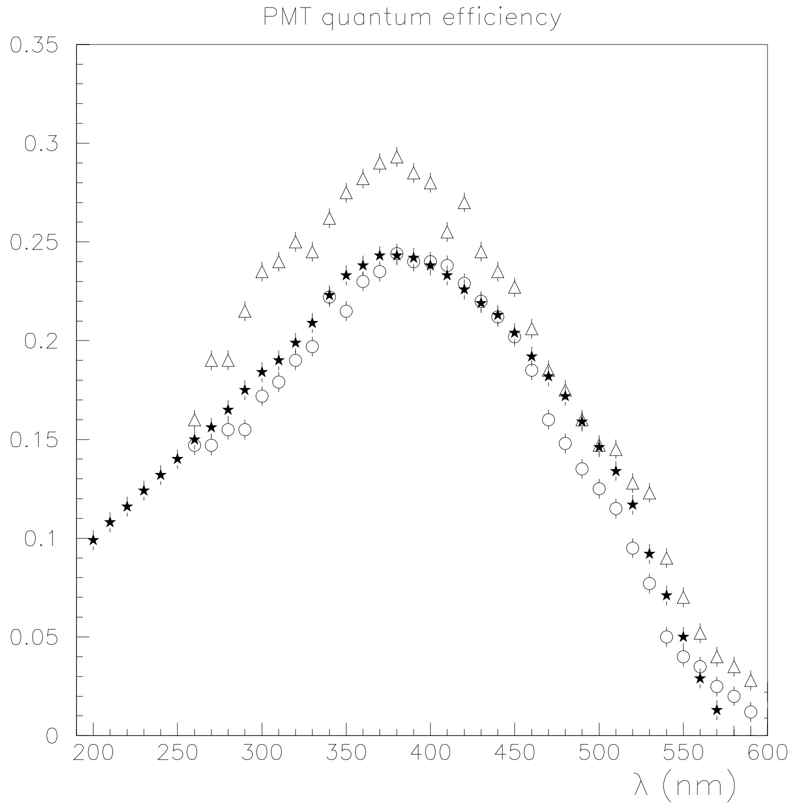

Figure 12: PMT quantum efficiency.

group of seven PMTs tested at CEBAF. The parameterization used in our simulation is in reasonable agreement with the measured data.

It is convenient to represent ν_γ in the form

$$\nu_\gamma = \nu_{init}\ (\varepsilon_{refl})^{N_{ref}}$$

where ν_{init} is the number of the emitted effective photons per 1 cm of electron trajectory, and ε_{refl} is the mirror reflectivity, which is applied during ray-tracing at every reflecting surface. We note, that $< N_{ref} > \approx 3$, and $< L_\gamma > \approx 1.5$ meter.

For C_4F_{10} gas and the new optics scheme these numbers are found to be

$$\nu_{init} = 0.737 cm^{-1}\ ,\ \varepsilon_{refl} = 0.793\ ,\ and\ \ \nu_\gamma = 0.368 cm^{-1}$$

The value of ν_{init} used in the particle detection efficiency calculations was reduced from previous estimations for Freon-12 gas and was set at $\nu_{init} = 0.44\ and\ \varepsilon_{refl} = 0.80$. The absolute accuracy of $N_{ph.e.}$ or ν_{init} is estimated at about 30% , therefore the figures shown can be considered as a conservative estimate.

All particle efficiencies were recomputed for C_4F_{10} gas and the modified geometry of the CLAS Čerenkov detector.

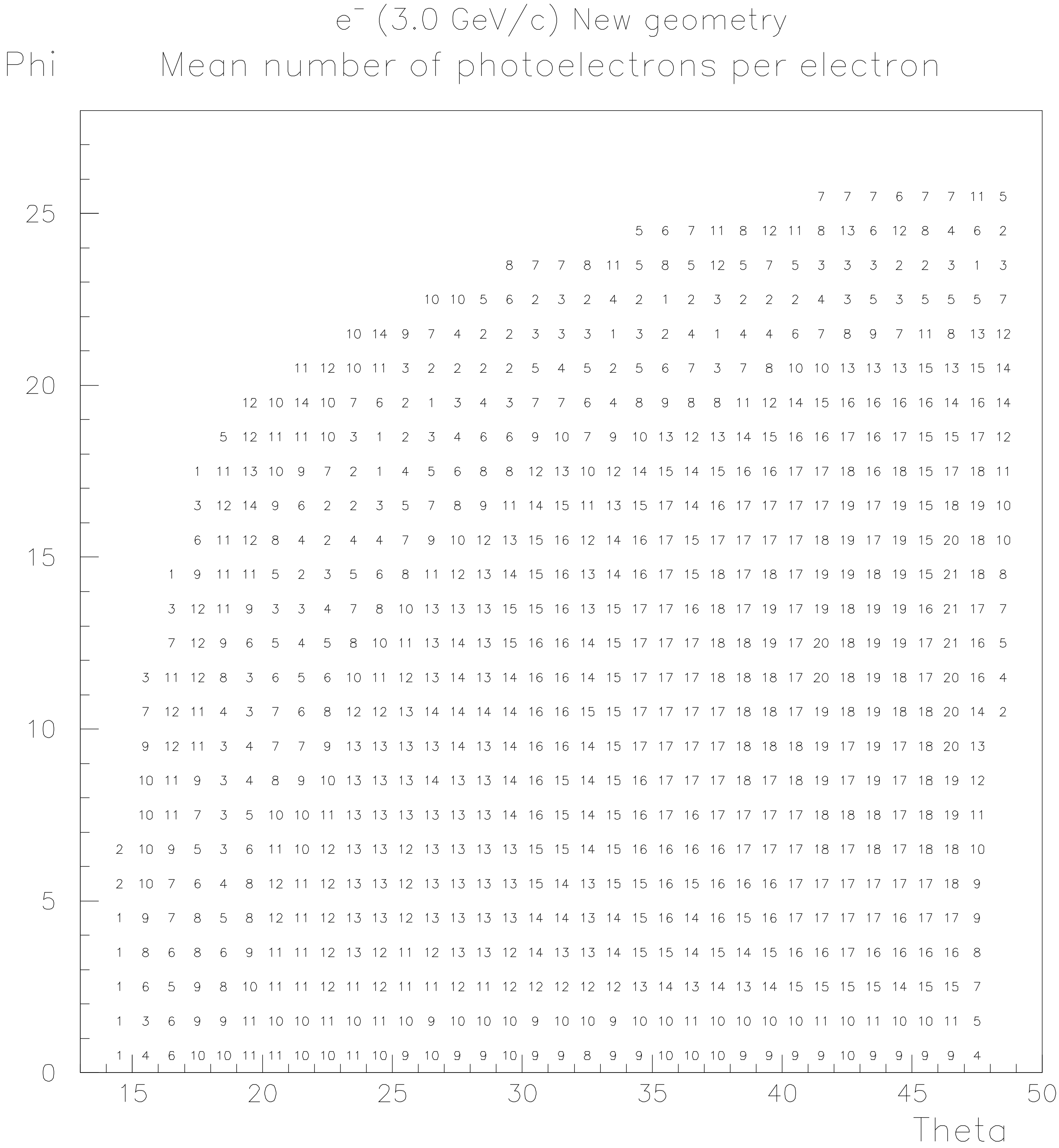

Figure 13: Mean number of photo-electrons

6.1 Electron efficiency

Fig. 13 shows the mean number of detected photoelectrons for 3.0 GeV electrons as a function of the polar angle *Theta* and the azimuthal angle *Phi*. It shows the angle range where electrons of a given energy can be detected with good detection efficiency (e.g. $N_{ph.e.} \geq 7$)

Detection efficiency is defined here as the ratio of the number of detected particles (here - electrons) to the number of particles entering the detector. Inefficiency is the deviation from the unity. Obviously, the particle detection efficiency depends on the applied threshold in terms of number of photo-electrons.

Fig. 14 and Fig. 15 show the electron inefficiencies for different detection thresholds : 1 and 3 photoelectrons respectively. A 3 photoelectron threshold means that the particle is assumed to be detected if there is at least one group of segments where the signal corresponds to 3 or more photoelectrons.

The number of generated events in each cell is $1500 \div 2000$, hence the accuracy of the simulation is about 0.1%.

Detection inefficiencies are less than 0.1% in most of the detected region for a *1 photoelectron* threshold, and less than 1% in case of a *3 photoelectron* threshold ($\approx$ 1% near the *middle plane*).

Fig. 16 and Fig. 17 show the electron inefficiency for energies of 1.8 and 0.8 GeV, respectively. One can see that the electron detection efficiency is rather independent of the incident electron energy.

6.2 Positron efficiency

Positrons, or electrons at reversed magnetic field polarity, can also be detected, although the range of angles is lower in this case.

Fig. 18 shows the mean number of detected photoelectrons for 1.8 GeV e^+ as a function of the segment number. Only about 50% of all segments are active. This is due to the strong magnetic field at small angles bending positrons away from the beam axis.

Fig. 19 shows the same value as a function of angles *Theta* and *Phi*. It can be seen that the detection efficiency near the *middle-plane* is smaller for e^+ than for e^-, however most of the remaining region has reasonable detection efficiencies for e^+.

6.3 Pion detection efficiency and π/e rejection

The threshold velocity v for particles to produce Čerenkov light is given by the index of refraction of the radiator gas. The corresponding γ values are shown in the Table 2. A typical value is $\gamma \approx 20$, corresponding to about 3 GeV/c pion momentum.

Unfortunately, sub-threshold pions can be also detected due to several mechanism :

- Slow particles can produce knock-on electrons (δ- electrons) with energies above threshold.

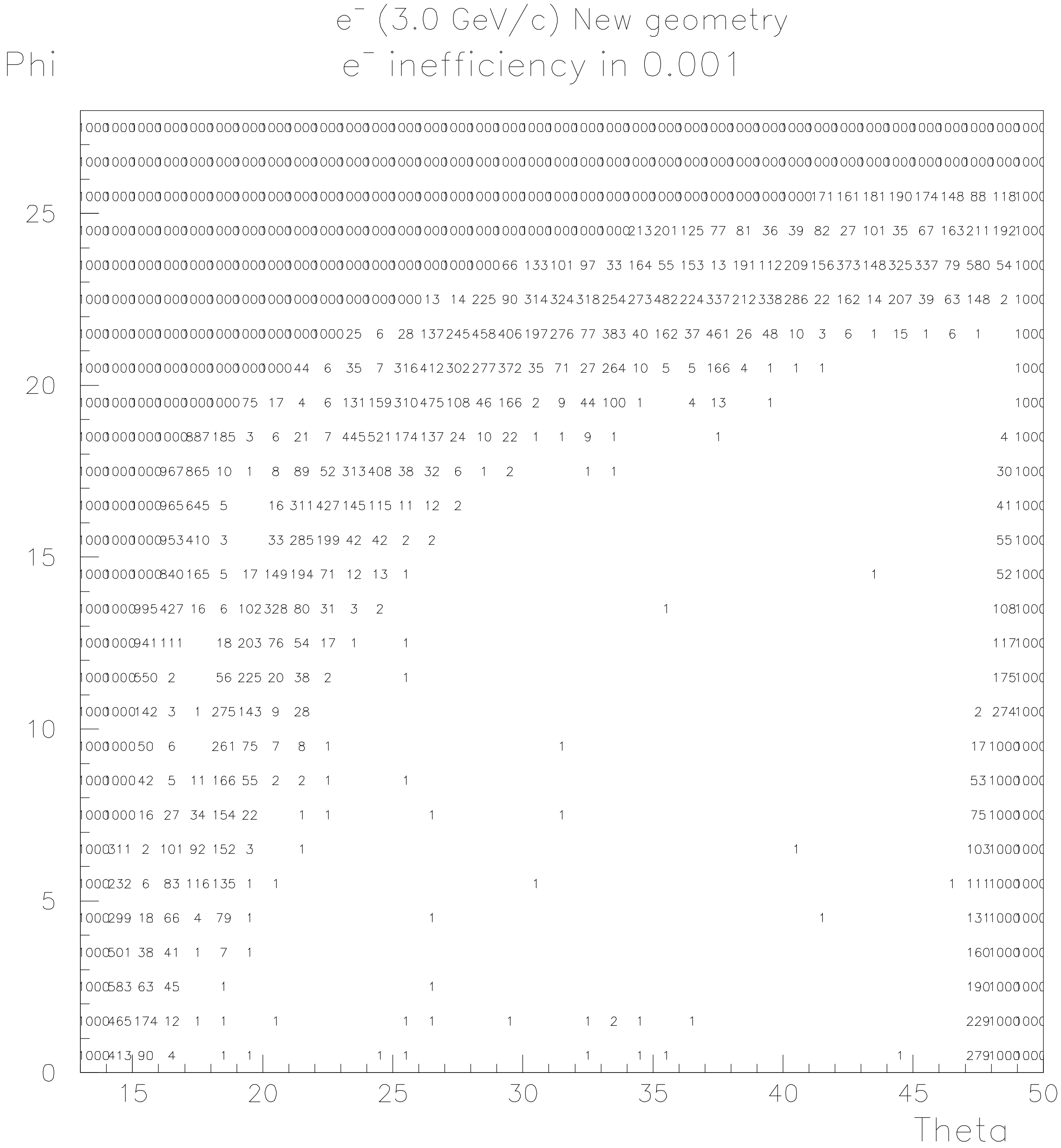

Figure 14: Electron inefficiency for 1 photo-electron threshold.

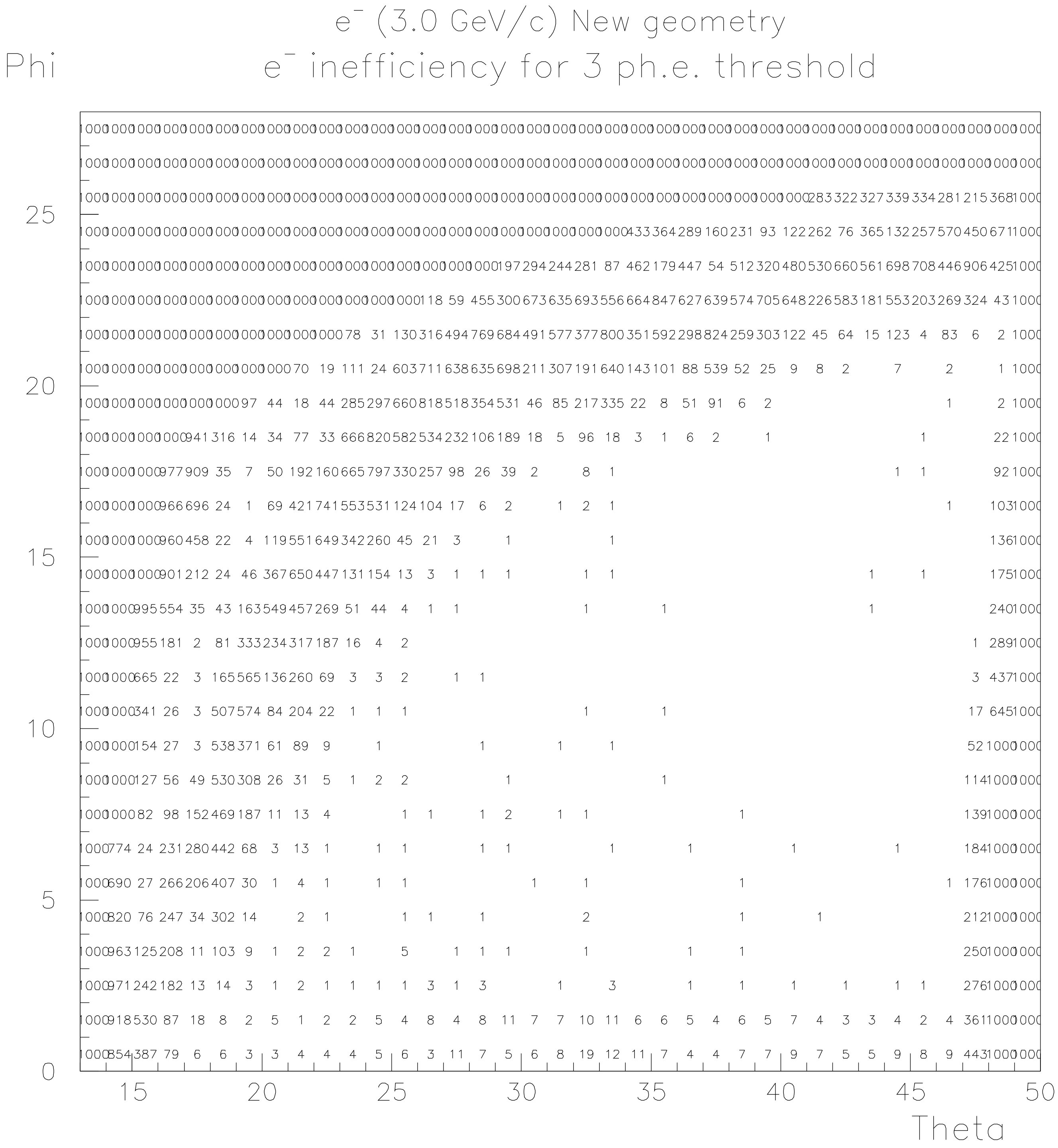

Figure 15: Electron inefficiency for 3 photo-electron threshold.

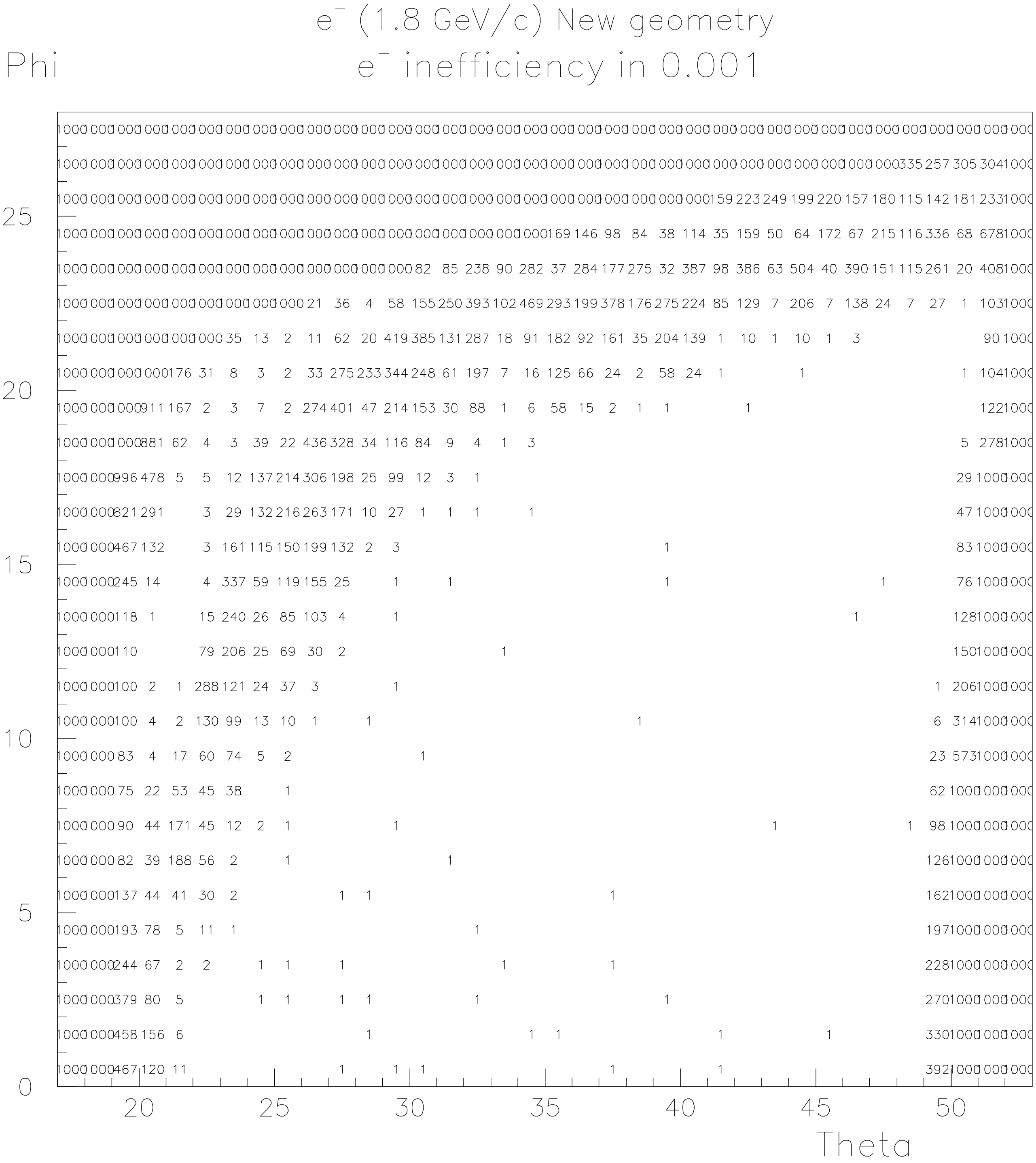

Figure 16: Electron inefficiency for 1 photo-electron threshold.

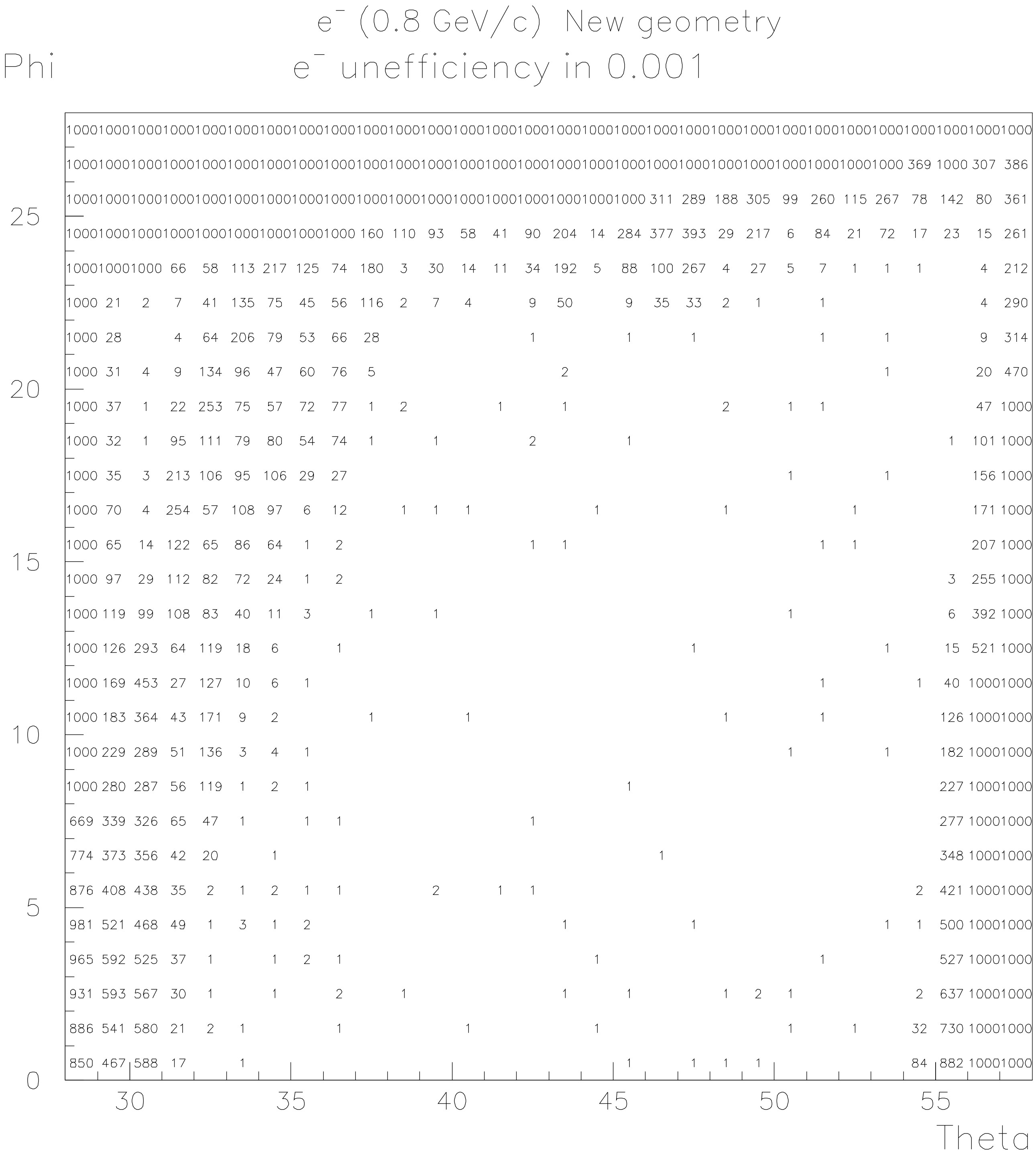

Figure 17: Electron inefficiency for 1 photo-electron threshold.

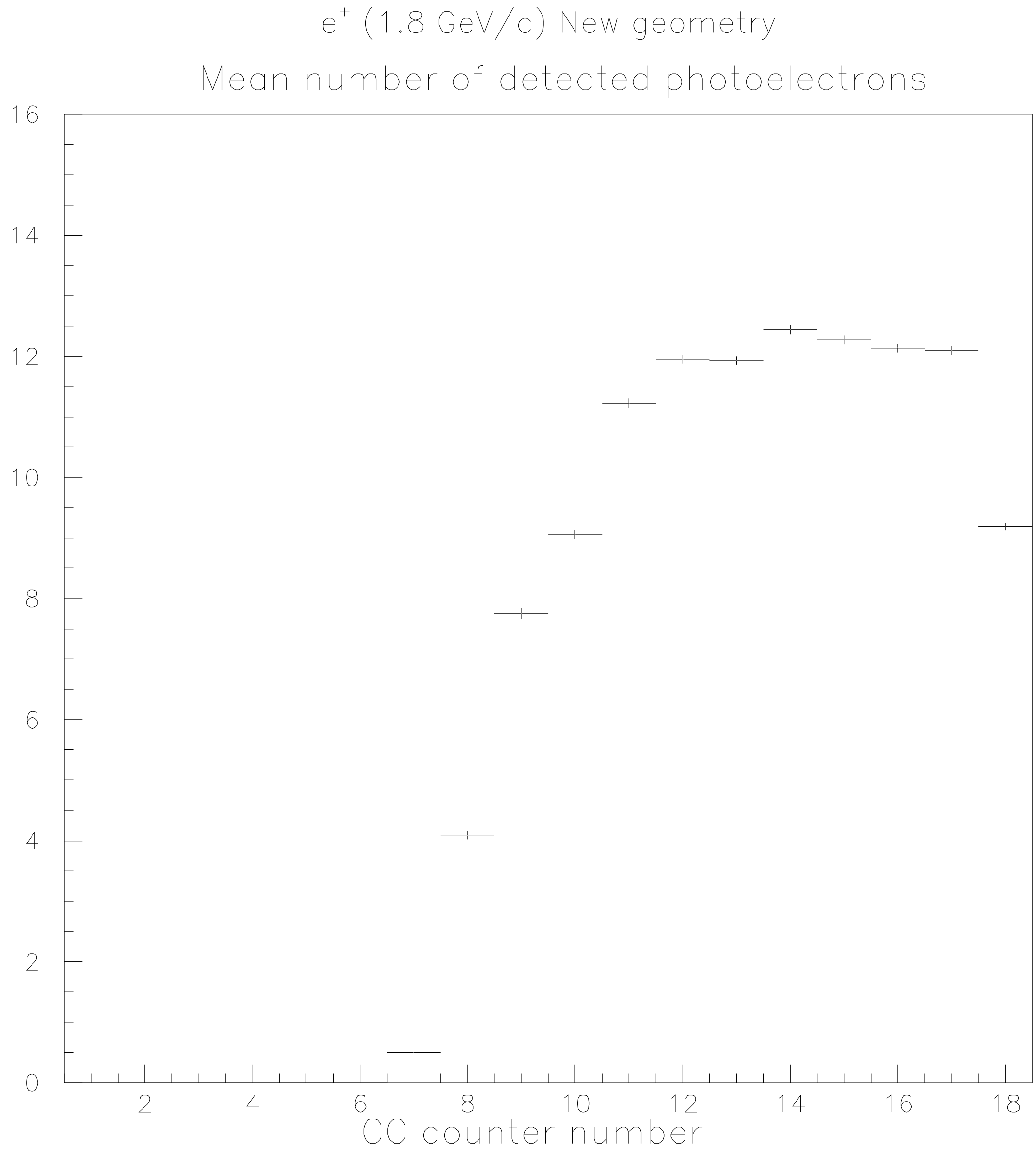

Figure 18: Mean number of photoelectrons for detected positrons as a function of the segment number.

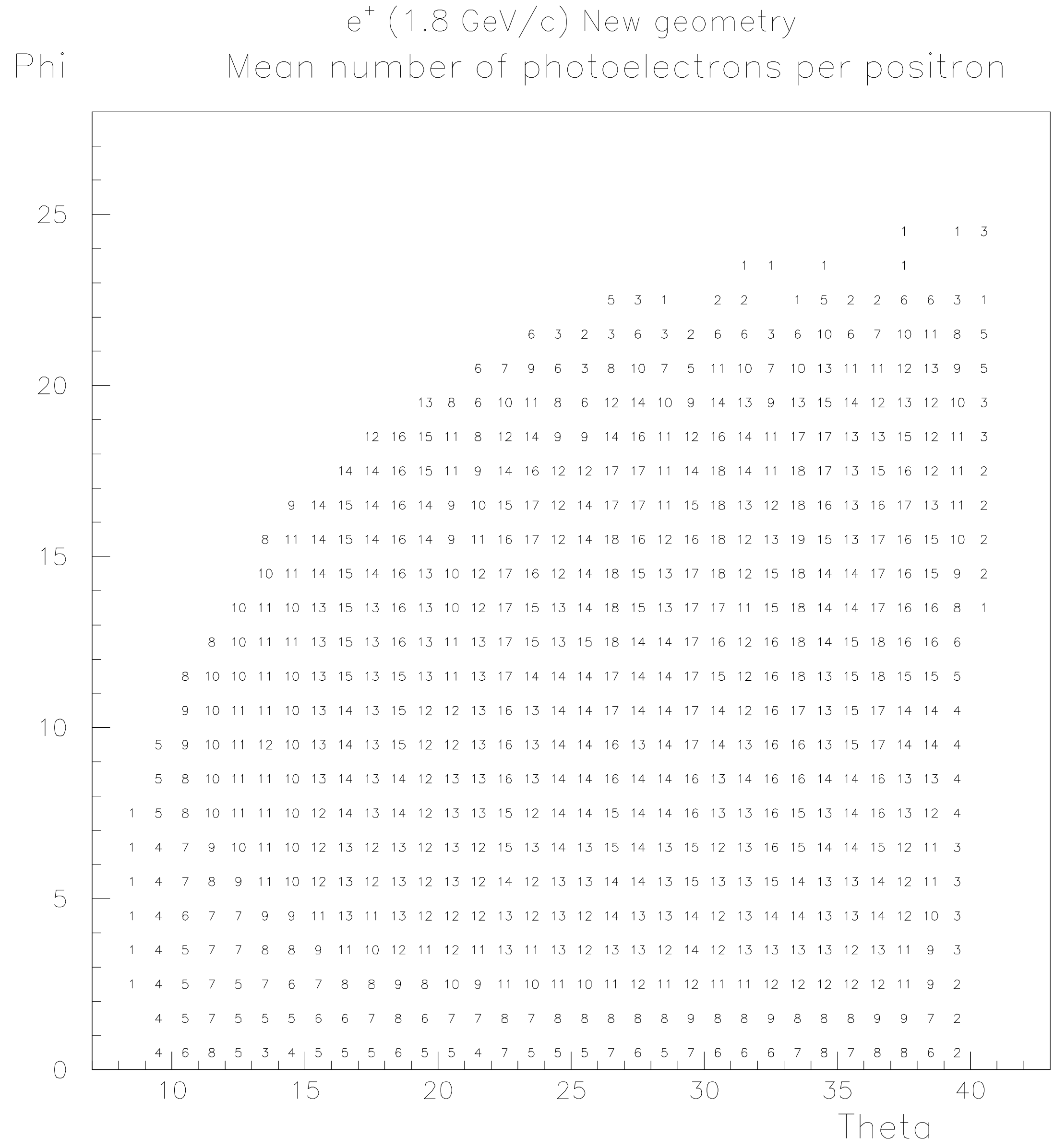

Figure 19: Mean number of detected photoelectrons as a function of polar (*Theta*) and azimuthal (*Phi*) angles.

- Nuclear reactions in the detector materials (mirrors, gas, magnetic shields and support frames) and in the materials in front of it (in drift chambers region) may produce secondary particles with velocities above threshold. An important contribution is pion charge exchange with π^o in the final state and subsequent conversion to γ - rays and electrons.

- In some gases, charged particles generate scintillation light, which can cause false Čerenkov signal.

The GEANT-based package appears adequate to accurately estimate the pion detection probability due to secondary particle production. It takes into account the important particle-nuclei interactions.

Fig. 20 represents the estimated π^- detection efficiency for three initial momenta : 0.8, 1.8 and 2.7 GeV/c, as a function of the CC segment number.

One can see that

- The pion detection probability increases with momentum. The mean probability for 0.8 GeV/c pions is $0.3 \div 1.0$ % , and for 2.0 GeV/c it is $1.0 \div 2.0$ %

- This probability is larger for smaller $Theta$ angles. This is likely a reflection of the higher material density at forward angles.

Full dots in the figure show the detection efficiency for π^- with momenta 10% above threshold. The efficiency is as low as $50 \div 60\%$. Quolitatively this is explained in the inserted graph in Fig. 20 - where the Čerenkov light intensity is plotted as a function of the π^- momentum. Pions with momenta 10% above threshold generate only about 10% of the light intensity of electrons. The π/e rejection can therefore be improved by setting higher detection threshold.

The π^+ detection probability was estimated for three different initial momenta - 2.7, 3.0 and 3.3 GeV/c for Freon-12 gas. (See fig. 21)

The threshold for Čerenkov light in this case is 3.0 GeV/c.

One can see that the difference in π^+ and π^- detection efficiencies is similar to the difference between e^+ and e^- : only about 50% of all segments are active in the case of π^+. The detection probability for the small angle segments is larger then for most others, however the number of events in this region is very small.

6.4 Photon detection probability and background estimations

Neutral particles, mostly photons , can also produce hits in the Čerenkov detector by e^+ e^- production near the sensitive detector volume. If a photon with energy $0.05 \div 0.2$ GeV converts to a e^+ e^- pair somewhere in the DC region, then these particles will not enter the detector if the magnetic field is sufficiently high. Therefore, materials near the detector are largely responsible for photon conversions and subsequent detection of an e^- or e^+.

Fig. 22 shows the probability for the detection of photons in the energy range $0.05 \div 0.2$ GeV, as a function of the segment number. The mean detection probability is about $1 \div 1.5\%$

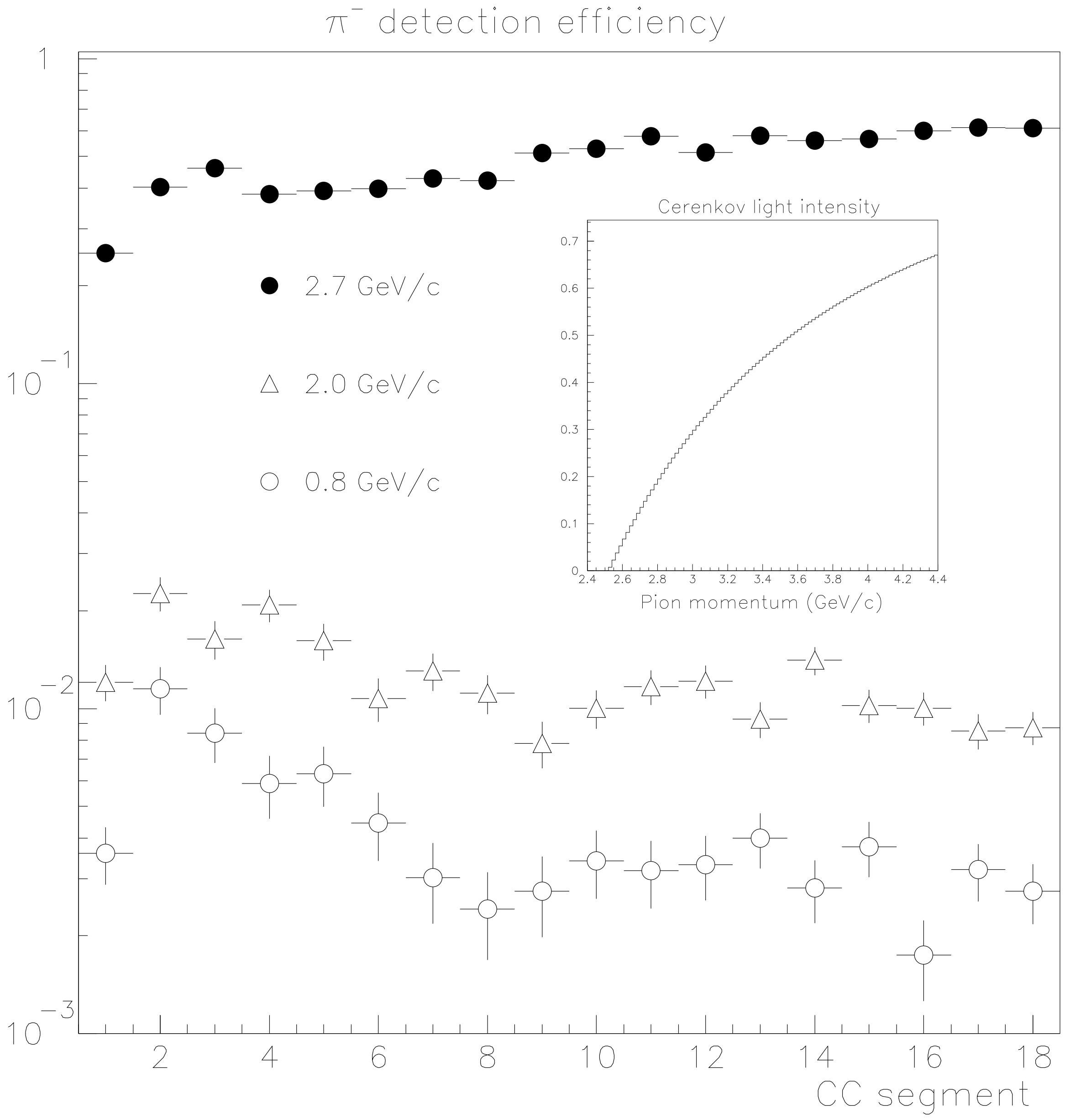

Figure 20: π^- detection efficiency

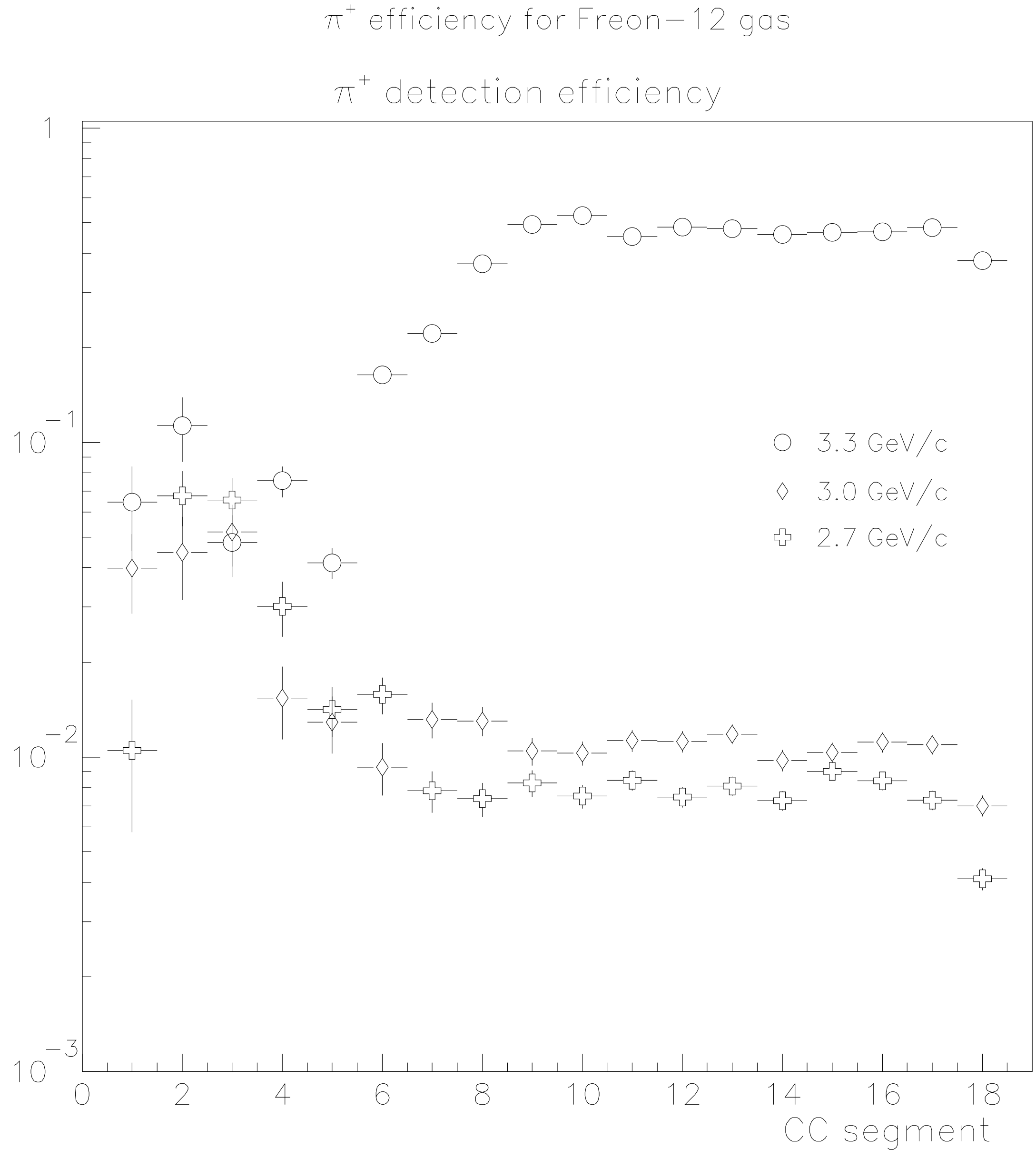

Figure 21: π^+ meson detection efficiency as a function of segment number.

for most of the effective region, and $2 \div 4\%$ for the small angle sections, where the material thickness is relatively large.

7 Summary

We can briefly summarize the improvements concerned Čerenkov detector:

- The new radiator gas - perfluorobutane (C_4F_{10}) is chosen. It is shown that this gas improves significantly the electron detection efficiency and has reasonable pion rejection (≈ 100).
- A new mirror is added to optimize the Čerenkov detector optics. It increases the number of detected photo-electrons and reduces the sensitivity to the deviation from the ideal mirror position.
- The Čerenkov detector optics is optimized for high and uniform electron detection efficiency.
- A procedure for the mirror alignment is developed. The sensitivity of the detection efficiency to the mirror position is investigated.
- Detection efficiencies for the the different particle types and energies are calculated.

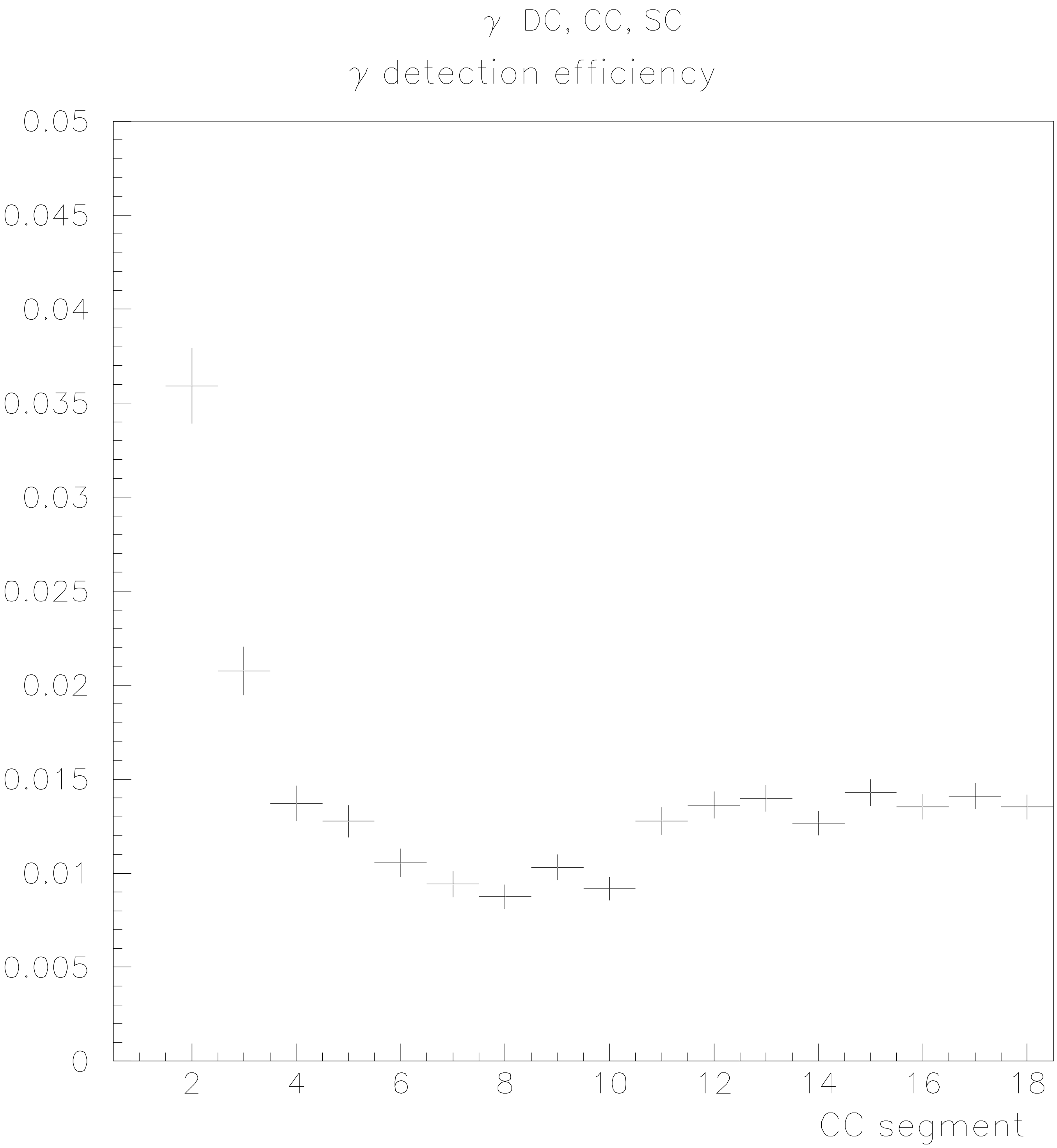

Figure 22: Photon detection probability.

References

[1] CERN Program Library Q123

[2] E. Doroshkevich, A. Vlassov, M. Kossov CLAS-NOTE **94-006** (1994)

[3] Particle data group

[4] Zrelov , Cherenkov radiation in high energy physics

[5] Jelley , Cerenkov radiation and it's application

[6] Nucl. Instr. and Meth. **138** (1976) p 641-646.

[7] Nucl. Instr. and Meth. in Phys. Res. **A248** (1986) p 118-129

[8] Nucl. Instr. and Meth. in Phys. Res. **A343** (1994) p 74-86.

[9] Nucl. Instr. and Meth. in Phys. Res. **A343** (1994) p 268-272.

[10] Nucl. Instr. and Meth. **93** (1971) p 593-594

[11] PCR Inc. P/O box 1466 Gainesville, Florida 32602 - 1466 phone (904) - 376 - 8246 Fax: 371-6246